ORIGINAL ARTICLE

Advanced Noise-Optimized Dual-Energy Virtual Monochromatic Imaging vs. Conventional 120-kVp CT Imaging: Image Quality Assessment

Adnan Honardari [1,2], Ahmad Bitarafan-Rajabi [3,4], Razieh Solgi [5], Mahsa Shakeri [1,2], Kiara Rezaei-Kalantari [6], Hossein Ghadiri [1,2,5] * ID

[1] Department of Medical Physics and Biomedical Engineering, School of Medicine, Tehran University of Medical Sciences, Tehran, Iran

[2] Research Center for Molecular and Cellular Imaging, Tehran University of Medical Sciences, Tehran, Iran

[3] Cardiovascular Intervention Research Center, Rajaie Cardiovascular Medical and Research Center, Iran University of Medical Sciences, Tehran, Iran

[4] Echocardiography Research Center, Rajaie Cardiovascular Medical and Research Center, Iran University of Medical Sciences, Tehran, Iran

[5] Preclinical Core Facility, Tehran University of Medical Sciences, Tehran, Iran

[6] Rajaie Cardiovascular Medical and Research Center, Iran University of Medical Sciences, Tehran, Iran

*Corresponding Author: Hossein Ghadiri
Email: h-ghadiri@tums.ac.ir

Abstract

Purpose: This study aimed at evaluating the image quality characteristics of advanced noise-optimized and traditional virtual monochromatic images compared with conventional 120-kVp images from second-generation Dual-Source CT.

Materials and Methods: For spiral scans six syringes filled with diluted iodine contrast material (1, 2, 5, 10, 15, 20 mg I/ml) were inserted into the test phantom and scanned with a second-generation dual-source CT in both single-energy (120-kVp) and dual-energy modes. Images set contain conventional single-energy 120-kVp, and virtual monochromatic were reconstructed with energies ranging from 40 to 190-keV in 1-keV steps. An energy-domain noise reduction algorithm was applied and the mean CT number, image noise, and iodine CNR were calculated.

Results: The iodine CT number of conventional 120-kVp images compared with monochromatic of 40-, 50-, 60- and 70-keV images showed increase. The improvement ratio of image noise on Advanced Virtual Monochromatic Images (AVMIs) compared with the Traditional Virtual Monochromatic Images (TVMIs) at energies of 40-, 50-, 60, 70-keV was 52.9%, 35.7%, 8.1%, 2.1%, respectively. At AVMIs from 75- to 190-keV, the image noise value was less than conventional 120-kVp images. CNR improvement ratio at 20 mg/ml of iodinated contrast material for TVMIs and AVMIs compared to 120-kVp CT images and AVMIs compared to TVMI was 18.3% and 56.3%, 32.1% respectively.

Conclusion: Both TVMIs (in energies ranging from 54 to 71-keV) and AVMIs (in energies ranging from 40 to 74-keV) represent improvement in the iodine contrast-to-noise ratio than conventional 120-kVp CT images for the same radiation dose. Also, AVMIs compared to TVMIs have been obtained considerable noise reduction and CNR improvement for low-energy virtual monochromatic images. In the present study, we show that virtual monochromatic image and its Advanced version (AVMI) may boost the dual-energy CT advantages by providing higher CNR images in the same exposure value compared to routinely acquired single-energy CT images.

Keywords: Dual-Source Computed Tomography; Dual Energy Computed Tomography; Advanced Virtual Monochromatic Images; Traditional Virtual Monochromatic Images; Contrast-to-Noise Ratio.

Frontiers in BIOMEDICAL TECHNOLOGIES

1. Introduction

Dual-Energy Computed Tomography (DECT) refers to the CT uses two x-ray spectrums (low- and high-energy) for collecting data sets. When various materials are simultaneously exposed by low- and high-energy x-ray photons, they show different attenuation coefficients. This attenuation coefficient change indicates the differences in physical interaction with low- and high-energy photons and resultant variations in the Compton and Photoelectric effects. There are several techniques to acquire DECT data, including dual-source, fast kVp switching, dual-layer detectors, dual-rotation, and twin-beam available from different vendors.

The first clinical DECT that is called Dual-Source CT (DSCT) became available in 2005 [1]. Dual-Source CT scanners using two almost orthogonally mounted x-ray tubes with corresponding detectors installed in the gantry of the scanner. Because of two separate x-ray tubes and detector sets, tube operation with different kilovoltage settings became attainable. DSCT is easy to use, improved radiation dose reduction technique, and several specific analyses such as visualization or subtraction of iodine and virtual monochromatic images compared to single-energy CT have made it an essential new emerging tool in daily practice. DECT techniques also have been shown practical clinical applications, such as virtual monochromatic imaging [2-5], iodine overly mapping [6-8], measurement of the effective atomic number [9, 10], and electron density [11] and nanoparticle-based molecular CT imaging to quantitative measuring of the contrast agent concentration [12].

Virtual Monochromatic Images (VMIs) are synthesized from dual-energy data set to simulate a scan acquired at the different monochromatic x-ray beams and the desired energy level. It can be used for diagnostic purposes similar to conventional single-energy images. VMIs are generated at a chosen kilo electron volt (keV) level without any additional radiation dose [13]. Typical energies have been ranging from 40 to 140 keV in different vendors and dual-source systems allowing up to 190 keV. VMIs at a low energy range (40-60 keV) are advantageous in improving Contrast-to-Noise Ratio (CNR) in contrast-enhanced CT studies, due to higher photoelectric attenuation as the energies approach the K-edge of iodine and result in enhancing lesion conspicuity. Improving the iodine signal is a promising future of dual-energy VMIs compared to conventional single-energy

images. However, VMIs at a low energy range that enhances the iodine signal also contain higher levels of noise which is a limiting factor in the clinical situations of Traditional Virtual Monochromatic Images (TVMIs) imaging. Currently, an Advanced noise-optimized Virtual Monochromatic Images (AVMIs) reconstruction algorithm has been introduced [15]. In the frequency domain, high-frequency information stands for noise and resolution, and low-frequency codes image contrast information. In this technique, a spatial frequency split approach is used, in which low-frequency information from the low-energy VMIs (with higher iodine contrast) is blended with high-frequency information from high-energy VMIs (with lower noise). The resulting images contain high contrast from low-energy VMIs and less noise due to high-energy VMIs. Therefore, VMIs contain less noise than the primary low-energy virtual monochromatic images. The improvement in image quality with the advanced noise-optimized algorithm is expected to be routinely used for suboptimal contrast enhancement [16], low iodine contrast uptake lesions, and reduction of metallic artefacts [17]. However, to the best of our knowledge, information on the suitability of advanced VMIs in comparison to traditional VMIs and conventional 120-kVp images for image quality such as noise and Contrast-to-noise ratio has not been reported.

The aim of the present study is to evaluate the effect of advanced noise-optimized VMIs on image quality characteristics in comparison to traditional VMIs and conventional 120-kVp images.

2. Materials and Methods

2.1. Phantom

For assessing image quality parameters, a test phantom [18] (a Teflon cylindrical phantom) in diameter and a height of 25 cm x 15 cm was scanned entirely (Figure 1).

Figure 1. Test phantom setup, including six syringes, containing diluted iodine enhancing material and ten distilled water syringes

In the present study, a total of sixteen cylindrical plastic syringes with diameter of 2.0 cm, and volume of 20 ml were placed into the phantom. Six syringes were filled with 1, 2, 5, 10, 15, 20 mg/ml of iodinated contrast material (Iohexol 300 (GE Healthcare)) to simulate the contrast-enhanced vascular structures. Each iodine concentration solution was added along with distilled water to the syringe. Ten plastic syringes containing distilled water were separately inserted into the phantom.

2.2. Image Acquisition and Reconstruction

Imaging was performed by a second-generation 2 x 64-slice dual-source CT (SOMATOM Definition Flash; Siemens Healthcare, Forchheim, Germany) in both single- and dual-energy modes. The test phantom was placed at the isocenter of the gantry to reduce unnecessary noise. Dual-energy images were obtained at 140 kVp with tin (Sn) filter as a high tube voltage (tube B) in combination with a low tube voltage (tube A) of 80 kVp in spiral scan mode. Tube currents for dual-energy scan were 261 mAs/ rotation at low tube voltage, and 101 mAs/ rotation at the high tube voltage. Single energy images were obtained at 120 kVp and tube current of 149 mAs/rotation. For a fair comparison of image quality between single- and dual-energy techniques, the radiation dose must be similar. This mAs was chosen to acquire DECT data sets at a comparable radiation dose for single energy mode. The mean CT dose index (CTDIvol) was 10.04 mGy for dual-energy scan and 10.08 mGy for single-energy. Before the scanning process, tube warming up and air calibration were performed. All acquisitions were repeated three times in the same scan range. The following scan parameters were used in both dual-energy and single-energy acquisitions: detector collimation, 64 x 0.6 mm in dual-energy mode, and 128 x 0.6 in single-energy mode; gantry rotation time 0.28 second; pitch factor, 0.5; and display Field-Of-View (dFOV), 30 cm. All images were reconstructed with a slice thickness of 1.0 mm, an increment of 1 mm, and an image matrix of 512 x 512 pixels, and thorax CT angiography medium smooth kernel (B31f). Also, Iterative Reconstruction (IR) and care dose 4D was switched off.

2.3. Image Analysis

All images were evaluated using a commercially available Siemens workstation Syngo. via software VB10A (Siemens Healthcare, Forchheim, Germany). VMIs (both TVMIs and AVMIs) were generated from 40- to 190-keV at 1.0-keV intervals by using commercial software (syngo Dual-Energy, version VA40; Siemens Healthcare) (Figure 2). Seven consecutive images from the middle of the phantom along the z-axis were selected for three scans, in total 21 images. The mean CT number and Standard Deviation (SD) were calculated separately using a 1.5 cm^2 circular Region Of Interest (ROI) for each diluted iodine contrast material and distilled water syringes in the test phantom. Image noise of background (SD water) was measured as the average value of the SD of mean CT number in ten distilled water inserts. Furthermore, CNR was calculated as follows (Equation 1):
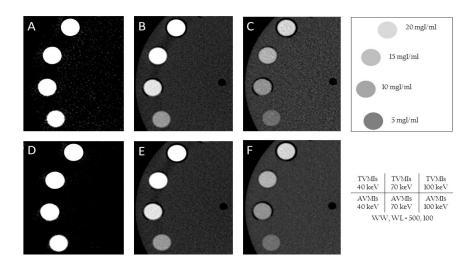
$$CNR = (ROI_{iodine} - ROI_{water}) / SD_{water} \qquad (1)$$

Figure 2. Virtual monochromatic images of the test phantom at, *A, D,* 40; *B, E,* 70; and, *C, F,* 100 keV at TVMIs and AVMIs images. The iodine concentrations at 5, 10, 15 and 20 mgI/ml were represented. The Window Width (WW) and Window Level (WL) were 500 HU and 100 HU

Where ROI_{iodine} was the mean CT number value of each iodine concentration, and ROI_{water} is the average mean CT number value of the distilled water. In addition, to compare CNR among the evaluated image series, the relative CNR (rCNR) was measured by dividing the CNR for each keV image (TVMI and AVMI) on the CNR for 120-kVp images [19] (Equation 2).

$$rCNR = CNR_{VMI} / CNR_{120-kVp} \qquad (2)$$

All statistical analyses were performed using GraphPad Prism software (Version 8.4.3; San Diego, California) and Microsoft Excel (2018). Differences in the mean CT values and image noise were analyzed using t-test. Variables were expressed as mean ± SD and P < 0.05 was considered to indicate a statistically significant result for the analyses performed.

3. Results

3.1. Iodine Mean CT Number

The mean CT number of 10 and 20 mg/ml iodine syringes on the TVMIs, AVMIs, and 120-kVp CT images are shown in Figure 3. The mean CT value difference of TVMIs and AVMIs at different iodine concentrations was not significant using t-test (all p > 0.05). The mean CT values of different diluted iodine concentrations in
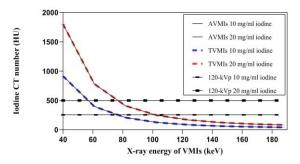

Figure 3. Mean CT number of 10 and 20 mg/ml iodine syringes on TVMIs, AVMIs and 120-kVp CT images. CT number were highest on 40-keV monochromatic images. As energy level of monochromatic images increased, the CT number of each syringe decreased

the 120-kVp images, TVMIs and AVMIs, are shown in Table 1. The iodine CT number of monochromatic of 40, 50, 60, and 70 keV images compared with conventional 120-kVp images showed an increase by approximately 3.6-, 2.4-, 1.6- and 1.2-fold. The mean CT values of the virtual monochromatic images were equal to those of the 120-kVp CT images at approximately 75-keV. The improvement ratio of mean CT value on the VMIs at 40 keV for 20 mg/ml iodinated material versus that on 120-kVp images shows an increase by 259.9% and 260.1%, respectively, for TVMIs and AVMIs (Table 1). The mean CT value improvement ratio was calculated with the following equation: (mean CT value of VMIs – mean CT value of 120-kVp) / mean CT value of 120-kVp.

Table 1. Mean CT number values of TVMIs, AVMIs and 120-kVp images at different iodine concentration

		Iodine Concentration					
		1 mgI/ml	2 mgI/ml	5 mgI/ml	10 mgI/ml	15 mgI/ml	20 mgI/ml
Traditional VMIs	**120-kVp**	23.0±0.6	51.1±1.3	125.0±1.2	256.7±1.3	369.9±1.0	499.7±2.1
	40-keV	80.3±3.6	182.1±4.1	446.9±3.1	914.3±3.2	1325.8±3.9	1798.3±5.2
	50-keV	54.0±1.9	120.3±2.2	294.5±1.7	601.9±1.6	873.2±2.3	1183.5±2.8
	60-keV	38.1±1.1	82.7±1.1	201.7±1.0	411.8±1.0	597.8±1.4	809.5±1.4
	70-keV	28.2±0.8	59.5±0.7	144.6±0.8	294.7±0.9	428.1±1.1	578.9±0.8
Difference between CT number of VMI at 40 keV and 120-kVp (%)		249.13	256.36	257.52	256.17	258.42	259.88
Advanced VMIs	**40-keV**	80.8±2.6	182.1±2.3	449.4±2.4	915.5±2.6	1328.7±3.2	1799.2±3.6
	50-keV	54.3±1.7	120.2±1.4	295.7±1.5	602.4±1.7	874.6±2.0	1183.7±2.2
	60-keV	38.1±1.1	82.6±0.9	202.1±1.0	411.9±1.1	598.4±1.3	809.4±1.4
	70-keV	28.2±0.8	59.4±0.6	144.5±0.7	294.4±0.8	428.1±1.0	578.5±0.9
Difference between CT number of VMI at 40 keV and 120-kVp (%)		251.30	256.36	259.52	256.64	259.21	260.06

Virtual monochromatic images of test phantom are shown in Figure 2 at 40, 70, and 100 keV at TVMIs and AVMIs images. However, the iodine signal is highest at 40 keV, the TVMIs images (Figure 2 A) markedly noisier.

3.2. Image Noise

Noise as a function of monochromatic energy levels (40- to 190-keV) is plotted in Figure 4. For simplicity, the results of conventional 120-kVp acquisition are shown here as a straight line. The image noise value for the conventional 120-kVp image was 12.6±0.8 HU. The noise on virtual monochromatic images depends on x-ray energy. At TVMIs, starting at 40-keV (61.9±2.4 HU) image noise quickly decreased; it reaches a minimum at 70-keV (13.7±0.5 HU) then increases more slowly as energy increases. At AVMIs, image noise shows significantly reduced at lower and higher image energies compared to the traditional VMIs, 29.1±1.2 HU, 8.0±0.3 HU at 40-keV,190-keV, $p<0.05$. Compared with the conventional 120-kVp images at TVMIs, the noise values at 68-keV to 72-keV energies are almost close to the 120-kVp images. At AVMIs from 75-keV to 190-keV (12.5±0.5 HU, 8.0±0.3 HU), the image noise value is less than conventional 120-kVp images. The improvement ratio of image noise on AVMIs Compared with the traditional VMIs at energies of 40-, 50-, 60, 70-keV was 52.9%, 35.7%, 8.1%, 2.1%, respectively (Table 2).
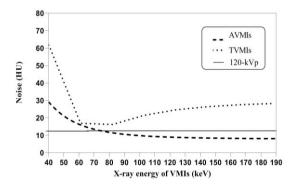

Figure 4. The mean noise of TVMIs, AVMIs and 120-kVp images. Mean noise on 120-kVp images was 12.6 HU. Image noise on TVMI images was lowest at 70-keV. Image noise on AVMIs from 75-keV was less than conventional 120-kVp images

3.3. CNR and Relative CNR

Figure 5 displays the mean CNR of 20 mg/ml iodine concentration on TVMIs and AVMIs from 40-190 keV range and 120-kVp CT images. The mean CNR

Table 2. Image noise (HU) at conventional 120-kVp, traditional virtual monochromatic and advanced noise-optimized virtual monochromatic images

	120-kVp	TVMIs	AVMIs
	12.6±0.8		
40-keV		61.9±2.4	29.1±1.2
45-keV		45.4±1.8	24.6±1.0
50-keV		32.8±1.4	21.1±0.9
55-keV		23.7±1.1	18.4±0.7
60-keV		17.7±0.8	16.3±0.7
65-keV		14.6±0.6	14.7±0.6
70-keV		13.7±0.5	13.4±0.5
80-keV		15.6±0.8	11.7±0.4
90-keV		18.4±1.0	10.5±0.4
100-keV		20.8±1.1	9.8±0.4
130-keV		25.2±1.3	8.7±0.3
160-keV		27.2±1.4	8.2±0.3
190-keV		28.3±1.4	8.0±0.3

values of 120-kVp images were 1.6, 3.8, 9.7, 20.1, 29.1, and 39.4 for contrast material concentrations of 1, 2, 5, 10, 15, 20 mgI/ml, respectively. On traditional VMIs, starting at 40-keV, iodine CNR first increased, reaching a maximum at 63-keV, and then decreased as the monochromatic energy increases further. CNR was considerably higher on TVMIs in the range of 54- to 71-keV (2.0, 5.0, 10.0, 15.0, 20.0 mgI/ml syringes) and 53- to 73-keV (1.0 mgI/ml syringe) compared with that on 120-kVp images. The highest CNR for each concentration of contrast material on AVMIs was obtained at 40-keV images than CNR gradually decreased as image energy increased. Table 3 shows the CNR on 120-kVp, 63-keV TVMIs and 40-keV AVMIs and the CNR improvement ratio of each image
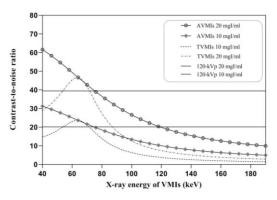

Figure 5. Mean CNR of 20 mg/ml idoine concentration on TVMIs, AVMIs from 40-190 keV range and 120-kVp CT images . The CNR for each diluated idoine syrnges was highest at 63-keV on TVMI images

Table 3. CNR of 120-kVp, 63-keV at TVMIs, 40-keV at AVMIs images and improvement ratios

Image type and improvement	Iodine concentration					
	1 mg/ml	2 mg/ml	5 mg/ml	10 mg/ml	15 mg/ml	20 mg/ml
120-kVp	1.6	3.9	9.7	20.2	29.1	39.4
63-keV TVMIs	2.0	4.6	11.5	23.6	34.4	46.6
40-keV AVMIs	2.6	6.1	15.3	31.3	45.4	61.6
TVMIs vs 120-kVp improvement ratio (%)	25.6	19.5	18.3	17.3	18.1	18.3
AVMIs vs 120-kVp improvement ratio (%)	60.1	57.6	57.1	55.1	56.0	56.3
AVMIs vs TVMIs improvement ratio (%)	27.4	31.9	32.7	32.2	32.1	32.1

types. Figure 6 shows relative CNR for 10 and 20 mgI/ml at TVMIs and AVMIs divided into CNR of 120-kVp images. Besides, relative CNR of AVMIs was almost 1.0 at 75-keV at 2, 5, 10, 15, 20 mg/ml iodine concentrations and at 81-keV in 1 mg/ml iodine concentration. The maximum CNR of virtual monochromatic images was shifted from 50- to 70-keV of the traditional VMIs to 40 at advanced noise-optimized VMIs, and the maximum CNR of AVMIs images is higher than both of TVMIs and conventional 120-kVp images.
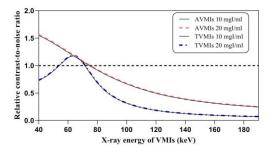

Figure 6. Relative CNR for 10 and 20 mgI/ml at TVMIs and AVMIs divided into CNR of 120-kVp images

4. Conclusion

DECT's unique post-processing facilities were used for commonly applied medical imaging techniques to improve medical diagnostics of all body areas [20]. In the past few years, in clinical situations, utilizing lower tube potentials in SECT (100-kVp) has been suggested to improve image quality and decrease radiation dose [21]. Nowadays, DECT and virtual monochromatic images have shown beneficial effects to increase CNR iodine

attenuation without the radiation dose penalty, so the CT values of the contrast agents steadily increased as well as image noise. This considerably increased image noise specially in lower monochromatic images has been a vital issue in the clinical situation [22]. In the present study, we investigated the performance of advanced noise-optimized VMIs algorithm and evaluated the CT value, image noise and CNR as the image quality characteristics of TVMI and AVMIs at different energy setting and compared to single-energy 120-kVp CT using second-generation DSCT.

Our results show the increased mean CT value on the TVMIs and AVMIs compared to 120 kVp images at lower energy (40, 50, 60 keV, p<0.05). Furthermore, the image noise increased considerably with lower monochromatic energy, and maximal CNR was obtained at 63-keV and was higher than 120-kVp single-energy CT. These results are in agreement with previous studies of VMIs using a dual-source CT scanner [23-25]. At advanced noise-optimized VMIs compared to traditional VMIs, significant noise reduction and CNR improvement have been shown that the specific amount of CNR improvement depends on the monochromatic energy level. Compared with TVMIs, noise reduction is more evident at the monochromatic energy lower than 60-keV and higher than 80-keV. Frellesen *et al.*'s finding shows that noise-optimized VMI reconstructions at the lowest available energy level of 40 keV resulted in more than thirty-fold increase in tumor CNR [23]. They also display when directly comparing the VMI and the noise-optimized VMI algorithms at the same keV levels, the noise-optimized VMI technique consistently showed reduced

background image noise, higher tumor SNR and CNR, and superior qualitative image quality results.

Our finding indicates that the maximum CNR of both TVMIs and AVMIs is higher than that of single-energy 120-kVp CT. In addition, at the equal contrast in AVMIs compared to TVMI, the CNR improvement is more significant at lower monochromatic energy, while noise is considerably reduced. Notably, the maximum CNR value of virtual monochromatic images is shifted from 63-keV for TVMI to 40-keV for AVMI. Grant et al. developed and investigated a new prototype monochromatic imaging algorithm (Mono+) that improved iodine CNR in images and decreased iodine concentrations using DECT at single-energy equivalent doses. Their results demonstrated that the modified monochromatic Mono+ technique provided increasing iodine CNR with decreasing keV for all phantom sizes, with the optimum CNR obtained at the lowest energy level of 40 keV [15].

The results show virtual monochromatic images are useful in clinical practice because they allow for reconstruction of images at several different energies (keVs) and therefore, also various contrast levels and image impressions from a single CT examination (exposure) [14, 15]. At low keVs, high-density materials, such as iodine, become very bright in the images and their contrast to the surrounding soft tissue increases [14]. Computing virtual monochromatic images at low keV from DECT data can potentially be considered an alternative to using low-tube voltages (low kVp) in CT scans with an iodinated contrast agent. In addition, the image noise can also be decreased by using advanced noise-optimized VMIs algorithm. AVMI shows increased iodine contrast at low keV without increased image noise, at a radiation dose level similar to conventional single-energy CT. Such an approach would potentially allow for a reduced amount of contrast material to be administered and thus reduce the risks of adverse events [15, 26-28].

Our study had several limitations. First, this study mainly focused on measuring image quality indices in the phantom to display the application of the advance noise-optimized virtual monochromatic images and did not discuss the effects on clinical situations. The second limitation was that only 120-kVp CT (in single-energy mode) images were compared. The third was that the information collection was based on seven consecutive images per scan which read by a person and might have permitted the possibility of bias.

In conclusion, both traditional and advanced virtual monochromatic images represent improved the iodine contrast-to-noise ratio than conventional 120-kVp CT images for the same radiation dose using dual-source dual-energy CT. Furthermore, advanced noise-optimized VMIs compared to traditional VMIs obtained considerable noise reduction and CNR improvement in low-energy virtual monochromatic images.

Acknowledgements

References

1- M. H. Albrecht, J.-E. Scholtz, J. Kraft, R. W. Bauer, M. Kaup, P. Dewes, et al., "Assessment of an advanced monoenergetic reconstruction technique in dual-energy computed tomography of head and neck cancer," *European radiology*, Vol. 25(8), pp. 2493-2501, 2015.

2- M. H. Albrecht, T. J. Vogl, S. S. Martin, J. W. Nance, T. M. Duguay, J. L. Wichmann, et al., "Review of clinical applications for virtual monoenergetic dual-energy CT," *Radiology*, Vol. 293(2), pp. 260-271, 2019.

3- P. Aspelin, P. Aubry, S.-G. Fransson, R. Strasser, R. Willenbrock, K. J. J. N. E. J. o. M. Berg. "Nephrotoxic effects in high-risk patients undergoing angiography," *New England Journal of Medicine*, Vol. 348(6), pp. 491-499, 2003.

4- C. Frellesen, M. Kaup, J. L. Wichmann, K. Hüsers, J.-E. Scholtz, M. H. Albrecht, et al., "Noise-optimized advanced image-based virtual monoenergetic imaging for improved visualization of lung cancer: comparison with traditional virtual monoenergetic imaging," *European Journal of Radiology*, Vol. 85(3), pp. 665-672, 2016.

5- U. P. Fulwadhva, J. R. Wortman, A. D. J. R. Sodickson. "Use of dual-energy CT and iodine maps in evaluation of bowel disease," *Radiographics*, Vol. 36(2*), pp. 393-406, 2016.

6- H. Ghadiri, A. Rahmim, M. Shiran, H. Soltanian-Zadeh, M. Ay, editors. A fast and hardware mimicking analytic CT simulator. *2013 IEEE Nuclear Science Symposium and Medical Imaging Conference (2013 NSS/MIC)*; 2013: IEEE.

7- M. K. Gill, A. Vijayananthan, G. Kumar, K. Jayarani, K.-H. Ng, Z. J. Q. i. i. m. Sun, et al., "Use of 100 kV versus 120 kV in computed tomography pulmonary angiography in the detection of pulmonary embolism: effect on radiation dose and image quality," *Quantitative imaging in medicine surgery*, Vol. 5(4), pp. 524, 2015.

8- K. L. Grant, T. G. Flohr, B. Krauss, M. Sedlmair, C. Thomas, B. J. I. r. Schmidt. "Assessment of an advanced image-based technique to calculate virtual monoenergetic computed tomographic images from a dual-energy examination to improve contrast-to-noise ratio in examinations using iodinated contrast media," *Investigative radiology*, Vol. 49(9), pp. 586-592, 2014.

9- T. R. Johnson, B. Krauss, M. Sedlmair, M. Grasruck, H. Bruder, D. Morhard, et al., "Material differentiation by dual energy CT: initial experience," *European radiology*, Vol. 17(6), pp. 1510-1517, 2007.

10- S. Khademi, A. Shakeri-Zadeh, R. Solgi, H. Azimian, H. J. I. N. Ghadiri. "Observation of targeted gold nanoparticles in nasopharyngeal tumour nude mice model through dual-energy computed tomography," *IET Nanobiotechnology*, Vol., pp., 2021.

11- D. Leithner, S. Mahmoudi, J. L. Wichmann, S. S. Martin, L. Lenga, M. H. Albrecht, et al., "Evaluation of virtual monoenergetic imaging algorithms for dual-energy carotid and intracerebral CT angiography: effects on image quality, artefacts and diagnostic performance for the detection of stenosis," *European journal of radiology*, Vol. 99, pp. 111-117, 2018.

12- L. Lenga, M. H. Albrecht, A. E. Othman, S. S. Martin, D. Leithner, T. D'Angelo, et al., "Monoenergetic Dual-energy Computed Tomographic Imaging," *Journal of thoracic imaging*, Vol. 32(3), pp. 151-158, 2017.

13- S. Lennartz, M. Le Blanc, D. Zopfs, N. Große Hokamp, N. Abdullayev, K. R. Laukamp, et al., "Dual-energy CT–derived iodine maps: use in assessing pleural carcinomatosis," *Radiology*, Vol. 290(3), pp. 796-804, 2019.

14- S. Mangold, C. Thomas, M. Fenchel, M. Vuust, B. Krauss, D. Ketelsen, et al., "Virtual nonenhanced dual-energy CT urography with tin-filter technology: determinants of detection of urinary calculi in the renal collecting system," *Radiology*, Vol. 264(1), pp. 119-125, 2012.

15- S. S. Martin, J. L. Wichmann, J.-E. Scholtz, D. Leithner, T. D'Angelo, H. Weyer, et al., "Noise-optimized virtual monoenergetic dual-energy CT improves diagnostic accuracy for the detection of active arterial bleeding of the abdomen," *Journal of Vascular Interventional Radiology*, Vol. 28(9), pp. 1257-1266, 2017.

16- S. Mashouf, E. Lechtman, P. Lai, B. Keller, A. Karotki, D. Beachey, et al., "Dose heterogeneity correction for low-energy brachytherapy sources using dual-energy CT images," *Physics in Medicine Biology*, Vol. 59(18*), pp. 5305, 2014.

17- C. H. McCollough, S. Leng, L. Yu, J. G. J. R. Fletcher. "Dual- and multi-energy CT: principles, technical approaches, and clinical applications," *Radiology*, Vol. 276(3), pp. 637-653, 2015.

18- F. G. Meinel, C. N. De Cecco, U. J. Schoepf, J. W. Nance Jr, J. R. Silverman, B. A. Flowers, et al., "First–arterial-pass dual-energy CT for assessment of myocardial blood supply: do we need rest, stress, and delayed acquisition? Comparison with SPECT," *Radiology*, Vol. 270(3), pp. 708-716, 2014.

19- S. R. Pomerantz, S. Kamalian, D. Zhang, R. Gupta, O. Rapalino, D. V. Sahani, et al., "Virtual monochromatic reconstruction of dual-energy unenhanced head CT at 65–75 keV maximizes image quality compared with conventional polychromatic CT," *Radiology*, Vol. 266(1), pp. 318-325, 2013.

20- M. Qu, G. Jaramillo-Alvarez, J. C. Ramirez-Giraldo, Y. Liu, X. Duan, J. Wang, et al., "Urinary stone differentiation in patients with large body size using dual-energy dual-source computed tomography," *European radiology*, Vol. 23(5), pp. 1408-1414, 2013.

21- E. D. Roele, V. C. Timmer, L. A. Vaassen, A. M. van Kroonenburgh, A. J. C. r. r. Postma. "Dual-energy CT in head and neck imaging," *Current radiology reports*, Vol. 5(5), pp. 19, 2017.

22- HS Thomsen, Contrast Media: Safety Issues and ESUR Guidline, Springer-Verlag (2006), ISBN 3-540-20448-2, Elsevier; p. 183, 2006.

23- D. Sakabe, Y. Funama, K. Taguchi, T. Nakaura, D. Utsunomiya, S. Oda, et al., "Image quality characteristics for virtual monoenergetic images using dual-layer spectral detector CT: comparison with conventional tube-voltage images," *Physica Medica*, Vol. 49, pp. 5-10, 2018.

24- D. Schneider, P. Apfaltrer, S. Sudarski, J. W. Nance Jr, H. Haubenreisser, C. Fink, et al., "Optimization of kiloelectron volt settings in cerebral and cervical dual-energy CT angiography determined with virtual monoenergetic imaging," *Academic radiology*, Vol. 21(4), pp. 431-436, 2014.

25- F. Stacul, A. J. van der Molen, P. Reimer, J. A. Webb, H. S. Thomsen, S. K. Morcos, et al., "Contrast induced nephropathy: updated ESUR contrast media safety committee guidelines," *European radiology*, Vol. 21(12), pp. 2527-2541, 2011.

26- A. J. van der Molen, M. C. J. A. J. o. R. Hovius. "Hematuria: a problem-based imaging algorithm illustrating the recent Dutch guidelines on hematuria," *American Journal of Roentgenology*, Vol. 198(6), pp. 1256-1265, 2012.

27- Y. Yamada, M. Jinzaki, Y. Tanami, T. Abe, S. J. I. r. Kuribayashi. "Virtual monochromatic spectral imaging for the evaluation of hypovascular hepatic metastases: the optimal monochromatic level with fast kilovoltage switching dual-energy computed tomography," *Investigative radiology*, Vol. 47(5), pp. 292-298, 2012.

28- L. Yu, J. A. Christner, S. Leng, J. Wang, J. G. Fletcher, C. H. J. M. p. McCollough. "Virtual monochromatic imaging in dual-source dual-energy CT: radiation dose and image quality," *Medical physics*, Vol. 38(12), pp. 6371-6379, 2011.